Spine Surgery and Related Research J-STAGE Advance Publication (March 11, 2024)

Clinical Significance Of Pose Estimation Methods Compared With Radiographic Parameters In Adolescent Patients With Idiopathic Scoliosis

Go Goto[1,2], Kousuke Ariga[3], Nobuki Tanaka[1], Kotaro Oda[1], Hirotaka Haro[1], Tetsuro Ohba[1*]

[1]Department of Orthopaedic Surgery, University of Yamanashi, Yamanashi, Japan

[2]National Hospital Organization Kofu National Hospital, Yamanashi, Japan

[3]Poslog Research, Poslog, Seattle, USA

*Address correspondence and reprint requests to:

Tetsuro Ohba

Department of Orthopaedics, University of Yamanashi

1110, Shimokato, Chuo, Yamanashi 409-3898, Japan

E-mail: tooba@yamanashi.ac.jp*

Phone: +81-55-273-6768

Fax: +81-55-273-9241

Acknowledgments: The manuscript submitted does not contain information about medical device(s)/drug(s). There are no pertinent financial activities beyond the scope of the submitted work.

Conflicts of Interest: The authors declare that there are no conflicts of interest.

IRB Statement: This study was approved by the institutional review board of the Yamanashi University (Approval No. 2556; February 2022).

Informed Consent: Written informed consent was obtained from the parents or guardians of all participants included in this study.

Spine Surgery and Related Research J-STAGE Advance Publication (March 11, 2024)

Clinical Significance Of Pose Estimation Methods Compared With Radiographic Parameters In Adolescent Patients With Idiopathic Scoliosis.

Abstract:

Background. Human pose estimation, a computer vision technique that identifies body parts and constructs human body representations from images and videos, has recently demonstrated high performance through deep learning. However, its potential application in clinical photography remains underexplored. This study aimed to establish photographic parameters for patients with adolescent idiopathic scoliosis (AIS) using pose estimation and to determine correlations between these photographic parameters and corresponding radiographic measures.

Methods. We conducted a study involving 42 patients with AIS who had undergone spinal correction surgery and conservative treatment. Preoperative photographs were captured using an iPhone 13 Pro mounted on a tripod positioned at the head of an X-ray tube. From the outputs of pose estimation, we derived five photographic parameters and subsequently conducted a statistical analysis to assess their correlations with relevant conventional radiographic parameters.

Results. In the sagittal plane, we identified significant correlations between photographic and radiographic parameters measuring trunk tilt angles. In the coronal plane, significant correlations were found between photographic parameters measuring shoulder height and trunk tilt and corresponding radiographic measurements.

Conclusions. The results suggest that pose estimation, achievable with common mobile devices, offers potential for AIS screening, early detection, and continuous posture monitoring, effectively mitigating the need for X-ray radiation exposure. **Level of Evidence:** 3.

Keywords: adolescent idiopathic scoliosis; pose estimation; posture parameters; deep learning; clinical photography; mobile applications; MoveNet; convolutional neural network

Introduction

Adolescent idiopathic scoliosis (AIS) is a structural and lateral curvature of the spine accompanied by rotation, affecting 1%–3% of children, typically manifesting around puberty[1]. Various radiographic parameters and classification methods are employed to diagnose and characterize scoliosis. The Cobb angle, the gold standard for detecting AIS and monitoring changes in spinal positioning, is critical for making decisions regarding surgery

or bracing. Additionally, shoulder and trunk imbalance are hallmarks of idiopathic scoliosis deformity[2–4]. Monitoring these aspects is crucial since alterations in posture can escalate the risk of psychosocial complications, including self-image, body image, mental health issues, and overall quality of life[5,6]. The Lenke classification is widely used to describe the scoliosis patterns, primarily organized by curve type (1–6) and a lumbar spine modifier (A, B, C)[7].

Timely screening and early detection of AIS are essential to prevent the progression of the deformity effectively. However, this poses challenges since mild scoliosis is typically asymptomatic, and access to X-ray machines is limited outside clinical settings. Additionally, for patients with AIS, repeated radiological assessments during follow-ups, which increase exposure to X-ray radiation, can increase the risks of developing conditions, such as leukemia, breast cancer, or a heritable defect beyond the baseline risk[8,9].

Many studies have investigated nonradiological methods of diagnosing body posture to reduce childhood exposure to X-ray radiation[10]. Some attempts have been made to assess patients with AIS using motion capture systems with markers on anatomical landmarks for medical examinations[11,12]. Although this method showed a correlation with radiographic measurements and good performance in detecting the progression of AIS, clinical application is still considered difficult because the method requires specialized equipment, such as reflective markers, and takes approximately half an hour per patient to conduct the measurement[13].

Additionally, clinical assessment through photography has gained popularity[13–17] due to its relative ease and cost effectiveness in evaluating trunk deformities[14,18]. For instance, shoulder balance determined by photographs of undressed patients is correlated with the clavicle angle[4]. Similarly, waistline asymmetry measurements and the ratio of the back area obtained through photographs of undressed patients correlate with the Cobb angle. The waist region measurements of undressed patients can identify the Lenke classification and are considered a valid method for assessing torso asymmetry in patients with severe AIS[14,19]. Clinical photographs have also been shown to be useful in assessing cervical spine balance in the sagittal plane[20]. In these studies, the images were not only taken with patients undressed,[11,15] but also required manual landmark measurements using software like ImageJ. However, this approach is time-consuming and prone to interobserver errors. Despite the potential value of clinical photography, consensus among surgeons remains undetermined regarding its use in preoperative assessment for determining spinal deformities[21].

In recent years, there has been growing interest in the image-based markerless motion capture method, commonly known as human pose estimation. Human pose estimation is a computer vision technique that identifies body parts and constructs human body representations from data like images and videos[22]. Human pose estimation eliminates manual work, thereby reducing the potential for intraobserver or interobserver errors. Another notable feature is that pose estimation operates entirely through software, making a common device, like a smartphone, sufficient for use. Moreover, popular pose estimation software is publicly available, effectively reducing installation costs to zero. The effectiveness of this method has significantly improved with the integration of deep learning[20], which leverages extensive datasets to enhance accuracy. While mobile applications employing pose estimation have become a valuable tool for evaluating posture, especially in

kinematics[23], the extent of its adoption in clinical evaluation remains a subject of debate[24,25]. Previous research has explored the accuracy of a pose estimation method using X-ray videos of marmosets, but the present study marks the first attempt to compare it with humans, particularly patients with AIS[26].

Numerous pose estimation methods exist, including OpenPose[27], MoveNet[28], and DeepLabCut[29], each with its trade-offs between the time and computational capacity required for execution and the accuracy of the results. Among these methods, MoveNet stands out for its ability to perform real-time motion capture on limited hardware resources, such as a smartphone. This accessibility enhances the use of motion capture in clinical and other settings[24,30]. Additionally, because MoveNet can run on a smartphone, patient data does not need to be sent to a remote server, which is advantageous from a privacy perspective. A prior study compared pose estimation methods and conventional marker-based optical motion capture. The findings indicated that MoveNet exhibits the lowest errors when measuring spatiotemporal gait parameters compared with other pose estimation methods[31].

Suppose photographic parameters obtained through pose estimation align with radiographic parameters. Then, it becomes feasible to conduct AIS screening, achieve early detection, and maintain continuous posture monitoring without subjecting patients to X-ray radiation. The present study aimed to (1) define the photographic parameters of patients with AIS using pose estimation outputs and (2) ascertain correlations between these photographic parameters and corresponding radiographic measures.

Materials and methods

The present study was approved by our institutional review board. Written informed consent was obtained from the parents or guardians of all participants included in the study.

2.1. Patient population

We examined the medical records of 42 patients with AIS with major TL/L curves (Lenke Type 5C) or MT curves (Lenke Type 1A) who underwent posterior spinal fusion surgery or conservative treatment between July 2022 and August 2023 at our university teaching hospital (Table 1). Their average age was 15.95 years, with a standard deviation of 2.30, and their average BMI was 18.87, with a standard deviation of 2.40. A total of 37 out of 42 patients were female. They were categorized according to the Lenke classification, with 24 patients classified as type 1A and 18 patients as type 5C.

2.2. Data acquisition

Photographs were captured using an iPhone 13 Pro mounted on a tripod without zoom and positioned at a distance equivalent to that from the patient to the X-ray tube head. The photographs were taken of the patients while wearing short sleeves and short pants (Figure 1). Photographs and X-ray images were captured simultaneously using a remote control. To ensure the camera's alignment with gravity, we maintained the camera's level in pitch and roll axes. Measures were implemented to limit any inclination within a deviation

range of 0.5°, utilizing the iPhone's built-in three-axis accelerometer.

2.3. Pose estimation

Our study employed the MoveNet deep learning model for pose estimation[28,32]. Among the publicly available deep learning models tailored for real-time pose estimation on mobile devices, MoveNet stands out due to its optimization for movement and fitness activities. This optimization extends its applicability to various movement assessment tasks. MoveNet takes RGB images as input and outputs x and y coordinates for 17 distinct body landmarks, including the nose, left and right eyes, ears, shoulders, elbows, wrists, hips, knees, and ankles (Figures 2 and 3). A noteworthy feature of MoveNet is its ability to focus on an individual closest to the image center, effectively disregarding others in the background. The model was developed using two extensive datasets: the COCO Keypoint Dataset[33], encompassing images captured in diverse settings with variations in size and occlusions, and the Active Dataset[34], comprising images depicting individuals engaged in activities, such as exercise, stretching, or dancing, collected from YouTube. Collectively, these datasets incorporate 51,500 images.

To ensure optimal results, the input image provided to MoveNet should possess dimensions larger than 256 x 256 pixels. In our study, the iPhone Pro 13 met this requirement. Additionally, the decision not to utilize facial landmarks, including the nose, left and right eyes, and ears, to calculate photographic parameters is noteworthy. This decision was necessitated by the use of face masks by patients during COVID-19, compromising the precision of facial landmark localization.

2.4 Photographic parameters

We used a subset of the 17 points obtained through pose estimation to define five novel photographic parameters (Table 2). In the coronal plane, we established the following parameters: Shoulder Height Angle (SHA), Hip Height Angle (HHA), and Coronal Trunk Tilt Angle (CTTA). In the sagittal plane, we introduced Sagittal Trunk Tilt Angle Shoulder-Hip (STTA_SH) and Sagittal Trunk Tilt Angle Ear-Hip (STTA_EH).

SHA is the angle formed between the line connecting the left and right shoulder points and the horizontal axis, and it is designed to quantify the balance of shoulder height. HHA is the angle formed between the line connecting the left and right hip points and the horizontal axis, indicating pelvic height balance. CTTA is the angle between the line connecting the middle of the shoulder and hip points and the vertical axis. STTA_SH is the angle between the line connecting the middle of the shoulder and hip points and the vertical axis. STTA_EH is the angle between the line connecting the middle of the ear and hip points and the vertical axis. CTTA is a parameter indicating trunk tilt in the coronal. STTA_SH, and STTA_EH are parameters indicating trunk tilt in the sagittal plane.

2.5. Radiographic parameters

We measured eight conventional radiographic parameters from standing whole spine posterior-anterior and

lateral standing radiographs. The coronal alignment parameters are clavicle angle (Cla-A), radiographic shoulder height (RSH), C7-central sacral vertical line (C7-CSVL), Cobb angle, and pelvic obliquity. The sagittal alignment parameters are trunk tilt angle (TTA)[35], sagittal vertical axis (SVA), and T1 pelvic angle (TPA)[36]. Cla-A and RSH reflect shoulder balance. C7-CSVL reflects trunk balance. Pelvic obliquity reflects pelvic balance. TTA, SVA, and TPA reflect trunk tilt.

Radiographic measurements were reported by two board-certified spine surgeons (GG and TO) to determine the interobserver error. The mean values of their measurements were used to calculate an intraclass coefficient of 0.932, indicating high interrater reliability.

2.6. Statistical analysis

Mean values are reported for continuous variables. We used Prism (version 8.0; GraphPad Software, La Jolla, CA) to calculate summary statistics. The parameters determined by radiography and photography in the sagittal or coronal plane were compared individually using Pearson correlation coefficients to investigate validity. Correlation coefficients from 0.00 to 0.25 indicate little to no relationship, from 0.25 to 0.50 fair, from 0.50 to 0.75 moderate-to-good, and above 0.75 good to excellent. Asterisks are used to indicate statistical significance ($p < 0.05$).

Results

3.1. Photographic parameters

The average photographic parameters for the participants are summarized in Table 3. In sagittal photographic measurements, the average STTA_SH was −3.34° (ranging from −7.62 to +2.66). The average STTA_EH was −0.28° (ranging from −4.99 to +5.20). In coronal photographic parameters, the average SHA was 0.026° (ranging from −4.09 to +4.39). The average HHA was 0.38° (ranging from −3.75 to +2.58). The average CTTA was −1.14° (ranging from −5.32 to +0.98).

3.2. Radiographic parameters

The average radiographic parameters for participants are summarized in Table 4. In sagittal radiographic measurements, the average TTA was −2.95° (ranging from −7 to +3). The average SVA was −22.33 mm (ranging from −77.06 to +52.04). The average TPA was 2.86° (ranging from −13 to +21). In coronal radiographic measurements, the average Cobb was 34.87° (ranging from 14 to 73). The average C7–CSVL was −8.47° (ranging from −55.88 to +22.86). The average Cla-A was −1.90° (ranging from −6 to +5). The average RSH was −10.15 (ranging from −28.87 to +24.20). The average pelvic obliquity was −0.90° (ranging from −6 to +3).

3.3. Correlations

The correlations between the photographic and radiographic parameters are summarized in Tables 5 and 6.

3.3.1. Coronal

Regarding shoulder balance, we observed a good to excellent correlation between SHA and Cla-A ($r = 0.84$, $P < 0.0001$) and RSH ($r = 0.83$, $P < 0.0001$), respectively. No significant correlations were identified with other radiographic parameters.

Concerning pelvic balance, HHA correlated fairly with pelvic obliquity ($r = 0.40$, $P = 0.0079$) and a moderate-to-good correlation with C7-CSVL ($r = 0.52$, $P = 0.0004$). No significant correlations were observed with other radiographic parameters (Figures 4 and 5).

Regarding trunk balance, CTTA correlated significantly with the radiographic parameter C7-CSVL ($r = 0.88$, $P < 0.0001$). No significant correlations were found with other radiographic parameters.

3.3.2. Sagittal

Concerning sagittal parameters, all photographic and radiographic parameters capture trunk tilt. Therefore, we compared every combination of radiographic and photographic parameters. A significant correlation was noted between TTA and the photographic parameters STTA_SH ($r = 0.64$, $P < 0.0001$) and STTA_EH ($r = 0.85$, $P < 0.0001$). Similarly, a significant correlation was identified between SVA and the photographic parameters STTA_SH ($r = 0.51$, $P = 0.0006$) and STTA_EH ($r = 0.60$, $P < 0.0001$). However, no significant correlations were observed between TPA and the photographic parameters STTA_SH and STTA_EH (Figures 4 and 5).

Discussion

Our study identified a statistically significant positive correlation between alignment parameters determined through clinical photography with pose estimation and those obtained via conventional radiography. These correlations were observed in the sagittal and coronal planes. To our knowledge, this study represents the first to establish such correlations in humans, particularly patients with AIS.

Over recent decades, several nonradiographic methods for scoliosis evaluation have been proposed[13]. In contrast, our fully automatic method utilizes a smartphone and pose estimation software, offering the advantage of assessing numerous photographic parameters that correlate with radiographic parameters in real-time without requiring patients to undress. This approach facilitates the automatic and instant assessment of shoulder and trunk imbalances in patients with AIS requiring surgical intervention, thereby eliminating the need for X-ray radiation exposure and reducing interobserver errors. However, given the specific attire comprising short sleeves and short pants in this investigation, further research is necessary to gauge the potential impact of ill-fitting garments on the method's accuracy.

It is important to note that, based on the current output of the pose estimation methods, photogrammetry cannot fully replace radiographs, particularly in assessing the Cobb angle, which remains the gold standard for AIS diagnosis. We observed that photographic parameters are highly correlated with radiographic parameters whose landmarks are relatively recognizable visually and close to the pose estimation landmarks but not with others.

Nevertheless, we anticipate that the quantity and accuracy of information obtained through photography will improve with advancements in pose estimation methods and datasets. The output information and its pose estimation accuracy largely depend on the dataset used with the method. Datasets have varying variables, including the camera viewpoints, the number of people in images, the posture, and the attire worn by the participant. For example, MoveNet uses the COCO dataset developed for general purposes and the Active Dataset developed for fitness purposes. Designing reliable photographic parameters with a tailored dataset for clinical photography with additional landmarks would be possible.

To assess the practicality of pose estimation in clinical settings, it is essential to conduct further evaluations involving large and diverse datasets. This study exclusively enrolled patients with AIS who regularly visited our hospital, resulting in a limited sample size of 42 individuals, all with a high average Cobb angle of 34.87°. Since important decisions, such as bracing, often pertain to patients with AIS with Cobb angles ranging from 20° to 30°, it is crucial to evaluate the effectiveness of our method in this specific subgroup. Additionally, for this method to become a viable screening tool, its performance should be assessed in individuals with minor curves and a healthy control group of children without AIS. Furthermore, as our study included exclusively Lenke types 5C or 1A patients, it is essential to evaluate the method's performance in a diverse patient population, including those with single, double, and triple curves. Finally, considering that the BMI of the patients in this study was consistently low, with an average of 18.87, it is important to investigate the accuracy of pose estimation in patients with high BMIs.

While the potential errors introduced using different mobile devices have not been extensively evaluated, similar results can be obtained with other mobile devices meeting the resolution requirements, i.e., 256 × 256 pixels.

In this study, we presented significant correlations between photographic and radiographic parameters despite limitations in the pose estimation method and available data. These findings suggest that photographic posture analysis using readily available mobile devices holds promise for AIS screening, early detection, and continuous posture monitoring while eliminating the need for X-ray radiation exposure. Future studies should include large sample sizes, encompassing control groups of children without AIS and a diverse range of patients with AIS, accounting for variations in Cobb angle, BMI, and the Lenke classification. Additionally, determining definitive threshold values based on parameters derived from pose estimation is challenging. Nevertheless, with the continuous evolution within deep learning and pose estimation, future advancements hold promise for the method's potential application in medical assessments and rehabilitation. Iterative studies leveraging updated datasets and technological progress will likely facilitate its integration into these domains.

References

1. Weinstein SL, Dolan LA, Cheng JC, et al. Adolescent idiopathic scoliosis. Lancet.

2008;371(9623):1527-37.

2. Labelle H, Richards SB, De Kleuver M, et al. Screening for adolescent idiopathic scoliosis: an information statement by the scoliosis research society international task force. Scoliosis. 2013;8: 17. eng

3. Kuznia AL, Hernandez AK, Lee LU. Adolescent idiopathic scoliosis: common questions and answers. Am Fam Physician. 2020;101(1):19-23.

4. Matamalas A, Bagó J, D'Agata E, et al. Reliability and validity study of measurements on digital photography to evaluate shoulder balance in idiopathic scoliosis. Scoliosis. 2014;9(1):23.

5. Freidel K, Petermann F, Reichel D, et al. Quality of life in women with idiopathic scoliosis. Spine. 2002;27(4):E87-91.

6. Ohba T, Goto G, Tanaka N, et al. Upper extremity skeletal muscle mass asymmetry exacerbated by shoulder imbalance in Lenke1A adolescent idiopathic scoliosis. J Clin Med. 2022;11(23):7117.

7. Lenke LG, Betz RR, Harms J, et al. Adolescent idiopathic scoliosis: a new classification to determine extent of spinal arthrodesis. J Bone Joint Surg Am. 2001;83(8):1169-81.

8. Goldberg MS, Mayo NE, Levy AR, et al. Adverse reproductive outcomes among women exposed to low levels of ionizing radiation from diagnostic radiography for adolescent idiopathic scoliosis. Epidemiology. 1998;9(3):271-8.

9. Ovadia D, Bar-On E, Fragnière B, et al. Radiation-free quantitative assessment of scoliosis: a multi center prospective study. Eur Spine J. 2007;16(1):97-105.

10. Labecka MK, Plandowska M. Moiré topography as a screening and diagnostic tool-a systematic review. PLOS ONE. 2021;16(12):e0260858.

11. Penha PJ, Penha NLJ, De Carvalho BKG, et al. Posture alignment of adolescent idiopathic scoliosis: photogrammetry in scoliosis school screening. J Manipulative Physiol Ther. 2017;40(6):441-51.

12. Aroeira RMC, Leal JS, Pertence AEM, et al. Non-ionizing method of screening adolescent idiopathic scoliosis in schoolchildren. Cien Saude Colet. 2019;24(2):523-34.

13. Leal JS, Aroeira RMC, Gressler V, et al. Accuracy of photogrammetry for detecting adolescent idiopathic scoliosis progression. Spine. 2019;19(2):321-9.

14. Bago J, Pizones J, Matamalas A, et al. Clinical photography in severe idiopathic scoliosis candidate for surgery: is it a useful tool to differentiate among Lenke patterns? Eur Spine J. 2019;28(12):3018-25.

15. Stolinski L, Kozinoga M, Czaprowski D, et al. Two-dimensional digital photography for child body posture evaluation: standardized technique, reliable parameters and normative data for age 7-10 years. Scoliosis Spinal Disord. 2017;12(1):38.

16. Yusuke Y, Hideki S, Sachiko K, et al. Waistline asymmetry is most affects self-image in patients with adolescent idiopathic scoliosis. J Spine Research. 2022;13(11):1177-85.

17. Yang S, Jones-Quaidoo SM, Eager M, et al. Right adolescent idiopathic thoracic curve (Lenke 1 A and B): does cost of instrumentation and implant density improve radiographic and cosmetic parameters? Eur Spine J. 2011;20(7):1039-47.

18. Heitz PH, Aubin-Fournier JF, Parent É, et al. Test-retest reliability of posture measurements in adolescents with idiopathic scoliosis. Spine. 2018;18(12):2247-58.

19. Matamalas A, Bagó J, D Agata E, et al. Validity and reliability of photographic measures to evaluate waistline asymmetry in idiopathic scoliosis. Eur Spine J. 2016;25(10):3170-9.

20. Jabbar KM, Gandomi F. The comparison of two corrective exercise approaches for hyperkyphosis and forward head posture: a quasi-experimental study. J Back Musculoskelet Rehabil. 2021;34(4):677-87.

21. Zuckerman SL, Cerpa M, Baum GR, et al. Surgeons lack of agreement on determining preoperative radiographic and clinical shoulder balance in adolescent and adult idiopathic scoliosis patients. Eur Spine J. 2021;30(3):661-7.

22. Zheng C, Wu W, Chen C, et al. Deep learning-based human pose estimation: a Survey. ACM Comput Surv. 2024;56(1):1-37.

23. Jo B, Kim S. Comparative analysis of OpenPose, PoseNet, and MoveNet models for pose estimation in mobile devices. TS. 2022;39(1):119-24.

24. Hopkins BCB. Validity of PostureScreen Mobile® in the measurement of standing posture. Brigham Young University; 2014.

25. Timurtaş E, Avcı EE, Mate K, et al. A mobile application tool for standing posture analysis: development, validity, and reliability. Ir J Med Sci. 2022;191(5):2123-31.

26. Kirkpatrick NJ, Butera RJ, Chang YH. DeepLabCut increases markerless tracking efficiency in X-ray video analysis of rodent locomotion. J Exp Biol. 2022;225(16):jeb244540.

27. Cao Z, Hidalgo G, Simon T, et al. OpenPose: realtime multi-person 2D pose estimation using part affinity fields. arXiv:181208008 [Internet]. 2019 May [cited 2023 Oct 17]. Available from: http://arxiv.org/abs/1812.08008

28. Next-Generation Pose Detection with MoveNet and TensorFlow.js. [cited 2023 Oct 17]. Available from: https://blog.tensorflow.org/2021/05/next-generation-pose-detection-with-movenet-and-tensorflowjs.html

29. Mathis A, Mamidanna P, Cury KM, et al. DeepLabCut: markerless pose estimation of user-defined body parts with deep learning. Nat Neurosci. 2018;21(9):1281-9.

30. Boland DM, Neufeld EV, Ruddell J, et al. Inter- and intra-rater agreement of static posture analysis using a mobile application. J Phys Ther Sci. 2016;28(12):3398-402.

31. Washabaugh EP, Shanmugam TA, Ranganathan R, et al. Comparing the accuracy of open-source pose estimation methods for measuring gait kinematics. Gait Posture. 2022;97: 188-95. eng.

32. LeCun Y, Bengio Y, Hinton G. Deep learning. Nature. 2015;521(7553):436-44.

33. Lin T-Y, Maire M, Belongie S, et al.: Microsoft coco: Common objects in context. Computer Vision–ECCV 2014: 13th European Conference, Zurich, Switzerland, September 6-12, 2014, Proceedings, Part V 13. 2014: 740-55.

34. MoveNet: Ultra fast and accurate pose detection model. [cited 2023 Oct 17]. Available from: https://tfhub.dev/google/movenet/singlepose/thunder/4

35. Arima H, Yamato Y, Hasegawa T, et al. Discrepancy between standing posture and sagittal balance during walking in adult spinal deformity patients. Spine. 2017;42(1):E25-30.

36. Protopsaltis T, Schwab F, Bronsard N, et al. TheT1 pelvic angle, a novel radiographic measure of global sagittal deformity, accounts for both spinal inclination and pelvic tilt and correlates with health-related quality of life. J Bone Joint Surg Am. 2014;96(19):1631-40.

386 **Figure Legends**

387 Figure 1. Method of obtaining clinical photographic and X-ray images simultaneously.

388 Figure 2. Pose estimation using MoveNet.

389 Figure 3. Method of evaluating photographic parameters.

390 Figure 4. Correlation between photographic and radiographic parameters in the sagittal plane. *$P < 0.05$

391 Figure 5. Correlation between photographic and radiographic parameters in the coronal plane. *$P < 0.05$

392

Spine Surgery and Related Research J-STAGE Advance Publication (March 11, 2024)

Figure 1
Method of taking photographs

Figure1

190x254mm (96 x 96 DPI)

Figure 2
Pose estimation methods using MoveNet®

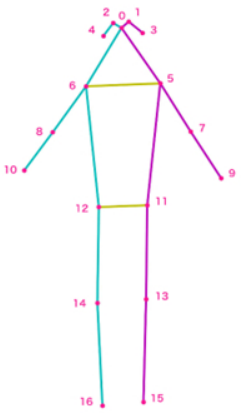

Number	Keypoint
0	Nose
1	L Eye
2	R Eye
3	L Ear
4	R Ear
5	L Shoulder
6	R Shoulder
7	L Elbow
8	R Elbow
9	L Wrist
10	R Wrist
11	L Hip
12	R Hip
13	L Knee
14	R Knee
15	L Ankle
16	R Ankle

L, Left; R, Right

Fig2

190x254mm (96 x 96 DPI)

Figure 3
Photographic parameters

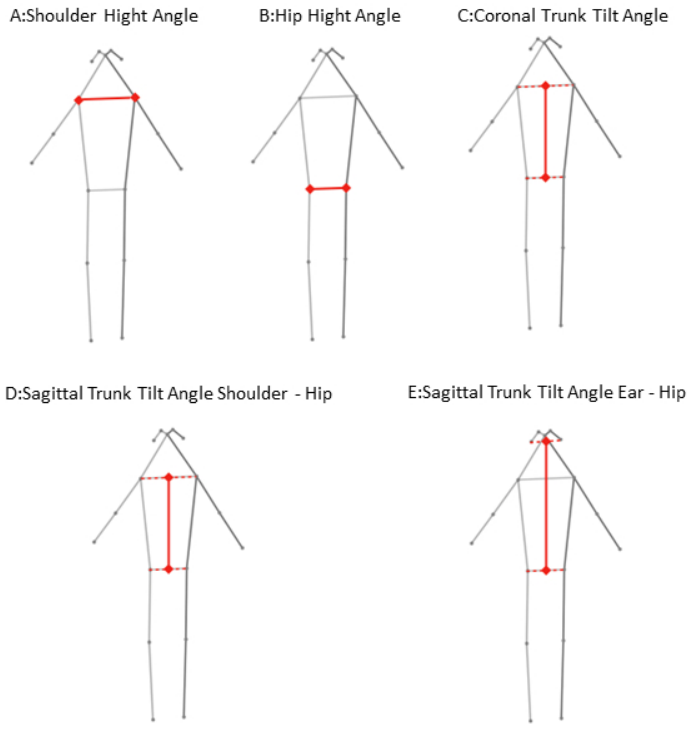

Figure3

190x254mm (96 x 96 DPI)

Figure 4
Correlation between radiographic and photographic parameters *$P < 0.05$

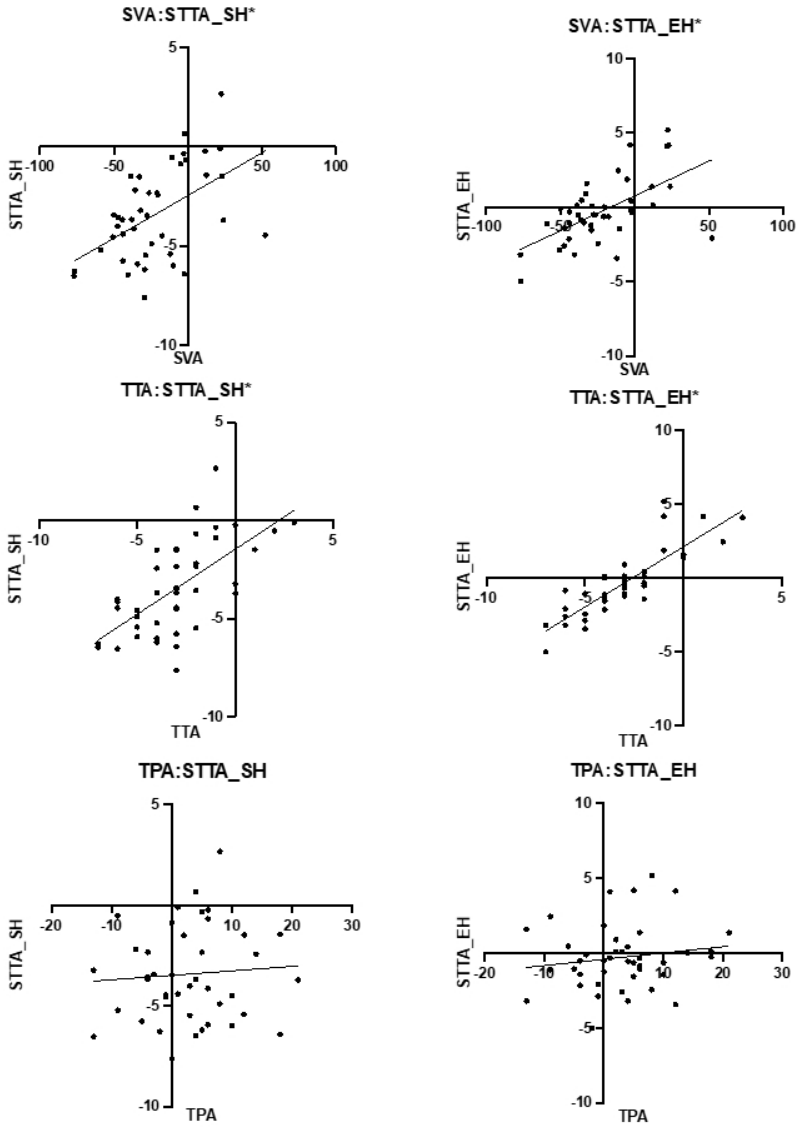

Figure4

190x254mm (96 x 96 DPI)

Figure 5
Correlation between radiographic and photographic parameters *$P < 0.05$

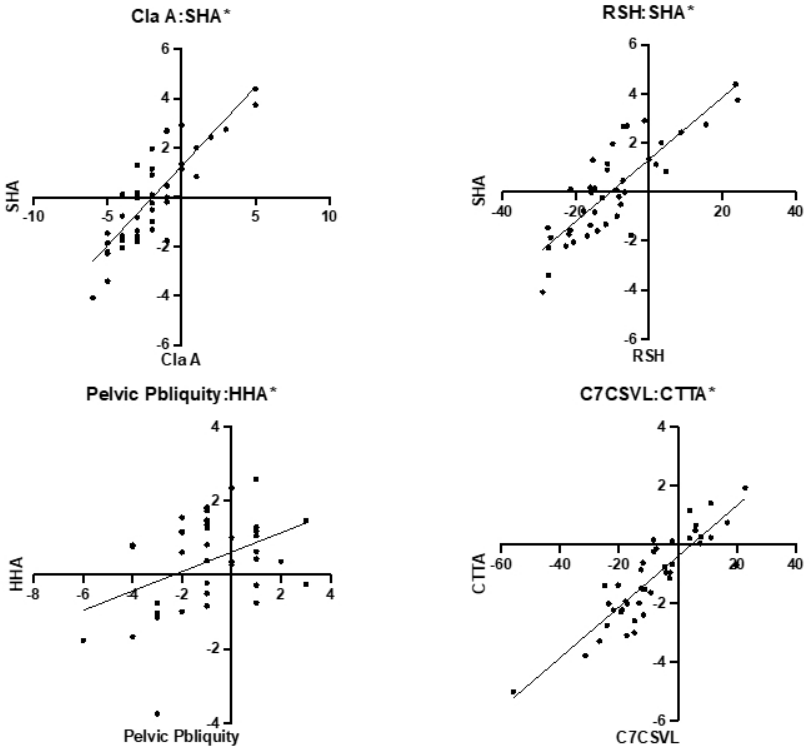

Figure5

190x254mm (96 x 96 DPI)

Spine Surgery and Related Research J-STAGE Advance Publication (March 11, 2024)

Table 1. Baseline characteristics of patients

	Average	Minimum	Maximum
Age	15.95 ± 2.30	2.30	12
BMI	18.87 ± 2.40	2.40	13.72
Sex	F:M	37:5	
Lenke	1A:5C	24:18	

Table 2. Photographic parameters

Segment			Plane		Pose estimation key points
Shoulder	Shoulder height angle	SHA	Coronal	A	The angle between each shoulder joint and a horizontal line
Hip	Hip height angle	HHA	Coronal	B	The angle between each hip joint and a horizontal line
Trunk	Coronal trunk tilt angle	CTTA	Coronal	C	The angle between the line connecting the midpoint of each shoulder with the midpoint of each hip joint and a vertical line
	Sagittal trunk tilt angle shoulder–hip	STTA_SH	Sagittal	D	The angle between the line connecting the midpoint of each shoulder joint with the midpoint of each hip joint and a vertical line
	Sagittal trunk tilt angle ear–hip	STTA_EH	Sagittal	E	The angle between the line connecting the midpoint of each ear with the midpoint of each hip joint and a vertical line

Table 3. Photographic parameters

	Average			Minimum	Maximum
Sagittal					
STTA_SH	−3.34	±	2.38	−7.62	2.66
STTA_EH	−0.28	±	2.15	−4.99	5.20
Coronal					
SHA	0.026	±	1.94	−4.09	4.39
HHA	0.38	±	1.27	−3.75	2.58
CTTA	−1.14	±	1.48	−5.32	0.98

STTA_SH, sagittal trunk tilt angle shoulder–hip; STTA_EH, sagittal trunk tilt angle ear–hip; SHA, shoulder height angle; HHA, hip height angle; CTTA, coronal trunk tilt angle;

Table 4. Radiological parameters

	Average	Minimum	Maximum
Sagittal			
TTA	−2.95 ± 2.27	−7	3
SVA	−22.33 ± 27.76	−77.06	52.04
TPA	2.86 ± 7.77	−13	21
Coronal			
Cobb	34.87 ± 12.36	14	73
C7-CSVL	−8.47 ± 15.16	−55.88	22.86
Cla-A	−1.90 ± 2.54	−6	5
RSH	−10.15 ± 12.71	−28.87	24.20
Pelvic Obliquity	−0.90 ± 1.96	−6	3

TTA, trunk tilt angle; SVA, sagittal vertical axis; TPA, T1 pelvic angle; Cobb, Cobb angle; C7–CSVL, C7–central sacral vertical line; Cla-A, clavicle angle; RSH, radiographic shoulder height

Table 5. Correlation between radiographic and photographic parameters

Sagittal		**STTA_SH**	**STTA_EH**
SVA (mm)	*r*	0.51	0.60
	P	**0.0006***	**<0.0001***
TPA (°)	*r*	0.07	0.15
	P	0.64	0.34
TTA	*r*	0.64	0.85
	P	**<0.0001***	**<0.0001***

TTA, trunk tilt angle; SVA, sagittal vertical axis; TPA, T1 pelvic angle; STTA_SH, sagittal trunk tilt angle shoulder–hip; STTA_EH, sagittal trunk tilt angle ear–hip

*$P < 0.05$

Table 6. Correlation between radiographic and photographic parameters

Coronal		**SHA**	**HHA**	**CTTA**
Cla-A	*r*	0.84	0.17	0.28
	P	**<0.0001***	0.29	0.074
RSH	*r*	0.83	0.14	0.28
	P	**<0.0001***	0.39	0.078
C7–CSVL	*r*	0.39	0.52	0.88
	P	**0.012***	**0.0004***	**<0.0001***
Pelvic Obliquity	*r*	0.10	0.40	0.46
	P	0.51	**0.0079***	**0.0019***
Cobb	*r*	−0.15	0.039	0.032
	P	0.33	0.80	0.84

Cobb, Cobb angle; C7–CSVL: C7–central sacral vertical line; Cla-A, clavicle angle; RSH, radiographic shoulder height; SHA, shoulder height angle; HHA, hip height angle; CTTA, coronal trunk tilt angle.

*$P < 0.05$